MOLECULAR RAMAN IN KXe

BY

KAVITA V. DESAI

THESIS

Submitted in partial fulfillment of the requirements
for the degree of Master of Science in Electrical and Computer Engineering
in the Graduate College of the
University of Illinois Urbana-Champaign, 2021

Urbana, Illinois

Advisors:

Professor J. Gary Eden
Research Assistant Professor Andrey E. Mironov

ABSTRACT

Stimulated Raman scattering in the KXe system has been observed for the first time. Stokes wavelengths were generated in the range of 770–770.5 nm. Mixtures of the K vapor and 300 Torr of Xe were pumped with 8 ns dye laser pumps in the range of 766-770 nm. Theoretical calculations confirm the observed experimental phenomena. It was also determined that it is possible to have gain in this system for the possible application of a tunable laser or amplifier.

To physics, for a never-ending field to explore.

ACKNOWLEDGMENTS

One of the greatest joys I have experienced in my education was the opportunity to interact with so many people throughout this journey. From all my teachers to the friends I have made I am entirely grateful. There are however some individuals that I would like to call out. First and foremost are my parents. From a young age, you always encouraged me to ask questions, learn about the world, and love learning. You also helped instill a love for numbers which has been very useful. The love and support you have given me is limitless. Next, of course, would be my fiancé Matt Kabelitz. You have given me endless support, love, and encouragement despite being 350 miles apart.

Gary, Andrey, and Christi, you all have inspired me to be the best researcher, engineer, and scientist. Gary, most people do not know that we met during my sophomore year in ECE 210. The passion you have for teaching and science radiates, and after all these years I always leave every conversation energized. You always believe in me and support every crazy idea I have in many ways. Andrey, the first time I met you was when you were subbing in ECE 455 talking about three and four level lasers. The enthusiasm and knowledge you have in this field is almost insane. You are always so approachable, helpful and friendly. Working with you is a privilege that I am grateful to have. Christi, if it weren't for you I do not think I would be in this lab. You sat me down in your office and talked to me like I was your own daughter. You saw a little spark in me and set me on fire. It's not always easy being a woman in this field, but you helped me gain confidence in myself and always continue to do so. You are a ray of sunshine in my life.

XPAL has been an ongoing project for a couple of decades. The previous graduate students and post-docs that worked on it discovered some incredible physics and engineered magnificent laser and amplifier systems. Sehyun, thank you for teaching me about this project and training me to take it

over. You are a brilliant engineer and friend, but what I miss the most about you is your smile and laugh. Stephen, I am so grateful to work on this system with you. You ask fantastic questions, and you are amazing at fixing the heater every time I do something wrong. Speaking of breaking things, here's another shoutout to Andrey who made the LabVIEW script and has incredible patience to debug it whenever it crashes.

Austin, you have become one of my closest friends and role models. You are an extremely gifted and talented lasercist, and you have taught me so much in the lab. You encourage my independence and confidence. Most importantly, the office pranks/shenanigans have been vital to my time here. Also, I just have to say, I beat you!

To all the other members of LOPE both past and present, you too have played an important role. I wish I had more space to acknowledge all of you, but I think I'll have to save it for a Murphy's happy hour.

TABLE OF CONTENTS

CHAPTER 1 INTRODUCTION 1

CHAPTER 2 EXPERIMENTAL SETUP 5

CHAPTER 3 RESULTS AND DISCUSSION 7
3.1 Transmission and ASE Scans 7
3.2 Pump-Probe and Excitation Scans 9
3.3 Molecular Raman 15

CHAPTER 4 CONCLUSIONS 19

APPENDIX A SUPPLEMENTAL DATA AND CALCULATIONS . . 21
A.1 Additional Experimental Data 21
A.2 Broadening Calculations 24

REFERENCES 25

CHAPTER 1

INTRODUCTION

Atomic alkali lasers have been of great interest over the past decades. These lasers when optically pumped on the D_2 resonance line, ($n^2P_{3/2} \leftarrow n^2S_{1/2}$, where n is 4, 5, 6 for K, Rb, and Cs respectively) can emit on the D_1 resonance line ($n^2P_{1/2} \rightarrow n^2S_{1/2}$) with a high quantum efficiency of over 90% [1]. An energy diagram for K is shown in Figure 1.1.

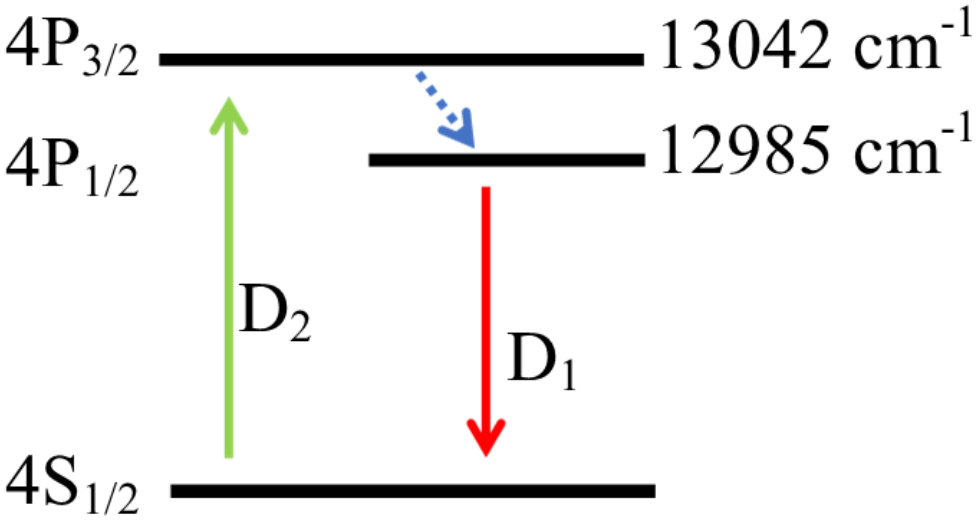

Figure 1.1: Energy level diagram for K. The 4^2P state energies where obtained from NIST [2].

While in theory, all the alkali metals can be used as laser gain media, most of the research has been focused on Rb and Cs. Li and Na have quantum efficiency >99.8% which results in the laser collapsing into a two-level laser; thus, it is impossible to optically pump the D_2 line for emission on the D_1 line. One technique to obtain lasing on the D_1 line in Na is to pump on the blue satellite of the D_2 line of NaXe [3]. In this setup, both the D_2 and D_1

line radiate unlike when pumping on the blue satellite of Rb or Cs. This technique to the best of our knowledge has not been applied to Li.

K on the other hand has a quantum efficiency of 99.6% when pumping on the D_2 line and having emission on the D_1 line, as can be observed in Figure 1.1. The high quantum efficiency of this system has been of great interest. The first D-line K laser was engineered in 2007 where 500 Torr of ethane was used as the buffer gas and the pump was a narrowband titanium sapphire laser [4]. It was found that the gain of K was 6% of Cs in the same system and the slope efficiency was only 20% [4]. Following that, a K laser with 2-3 atm of He has been engineered to have a similar slope efficiency to Rb at 64% but with a higher threshold [5]. A diode pumped K laser with 600 Torr He was also engineered to operate in the pulsed regime with 30 µs triangular pulses at 100 Hz repetition rate having a slope efficiency of 52% [6]. Due to the small separation distance between the D_2 and D_1 line of 57.7 cm^{-1} the threshold energy/power for this system is high compared to Rb and Cs.

One technique which could improve this system is to form a transient molecule in K with a rare gas and excite the alkali-rare gas molecule at a satellite structure. This molecule would then dissociate and the population inversion on the upper state in K would be easier to achieve. This method of pumping an excited dimer or excimer at a satellite structure (a more appropriate term for this would be an excited complex or exciplex, but in literature, the word excimer is used interchangeably) for an alkali-rare gas laser is known as XPAL, an excimer pumped alkali laser, which was first demonstrated at the University of Illinois by Readle *et al.* [1].

To the best of our knowledge, there has not been an XPAL laser made with K nor has a blue satellite of the D_2 resonance for a K-rare gas molecule been discovered. In this thesis, the original goal was to determine if KXe, where the gas pressure was 300 Torr, could be used as an amplifier system in an XPAL system. However, at this pressure, no blue satellite was determined, but amplification on the D_1 line was observed by pumping the D_2 line. This amplification is through a molecular process and has not been previously achieved in other alkali-rare gas systems. More importantly, in these experiments stimulated molecular Raman scattering was observed, which is the first of its kind observed in a transient system. These generated wavelengths have the ability to be engineered into a laser system.

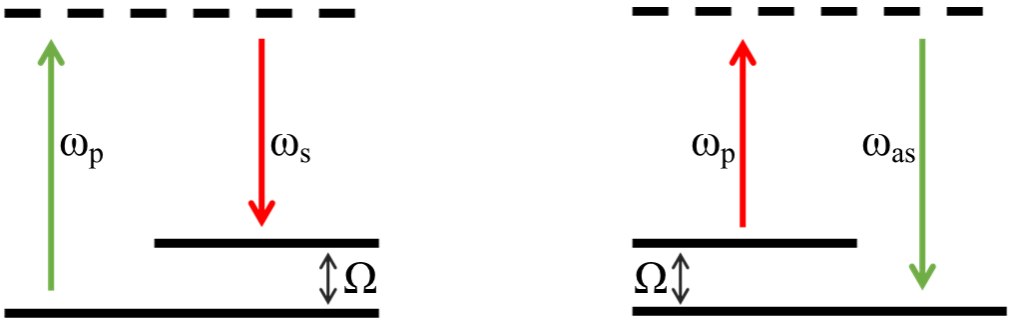

Figure 1.2: A simplified diagram of Stokes (left) and anti-Stokes (right) scattering where ω_p is the pump or incident wavelength and ω_s and ω_{as} are the scattering wavelengths for the Stokes and anti-Stokes processes. Ω is the energy separation between the pump and scattered wavelengths and the dashed horizontal line represents a virtual state.

Raman scattering is an inelastic scattering process, unlike Rayleigh scattering which is an elastic process. There are two categories of Raman scattering possible; Stokes and anti-Stokes scattering as shown in Figure 1.2. In Stokes scattering, the scattered light energy is less than the incident light; whereas in anti-Stokes scattering, the scattered light has a greater energy than the incident light. The latter of the two is less common. The incident light pumps to a virtual state which is a state that is only present with white light; this is not an intrinsic state of an atom or molecule.

Raman scattering can occur in both atoms and molecules and can be a stimulated process. In molecules, the term stimulated Raman scattering (SRS) is used to describe this process. Raman scattering in a molecule occurs from a change in polarizability from the molecules rotational or vibrational states [7]. Stimulated electronic Raman scattering (SERS), on the other hand, is for Raman scattering in electronic states in an atomic system. Both stimulated scattering methods are three photon processes where the nonlinear susceptibility is of the form $\tilde{\chi}^{(3)}_{ijkl}(\omega_s; \omega_p, -\omega_p, -\omega_s)$ where ω_p is the pump photon and ω_s is the scattered photon which can be from Stokes or anti-Stokes scattering. Another form of Raman scattering is hyper-Raman which is a five photon process where its nonlinear susceptibility is of the form $\tilde{\chi}^{(5)}_{ijklnm}(\omega_s; \omega_p, -\omega_p, \omega_p, -\omega_p, -\omega_s)$.

Stimulated electronic Raman scattering and hyper-Raman scattering have been observed in K atomic vapor. The first observation of SERS in K was

by Rokni and Yatsiv [8, 9] and Sorokin *et al.* [10] in 1967. The goal in these works was to generate longer wavelengths (Stokes scattering) [8–10] and shorter wavelengths (anti-Stokes scattering) [8] (in this particular experiment, the anti-Stokes line was due to parametric coupling). In 2013, similar experiments were conducted and three Raman processes were observed: Stokes and anti-Stokes SERS and hyper-Raman scattering [11].

One challenge for Raman scattering is that it is a weak process. One method is to increase the pump energy, which can potentially cause other nonlinear effects such as two-photon absorption or even ionization which could weaken the Raman scattering. Another method is to increase the nonlinear susceptibility, $\tilde{\chi}^{(3)}_{ijkl}(\omega_s; \omega_p, -\omega_p, -\omega_s)$, which is proportional to the inverse of the difference between the pump frequency and the resonance frequency. When operating near a resonance, the susceptibility grows significantly. In a quantum system, there are many resonances present which all also effect the nonlinear susceptibility in a similar manner. As a result, operating near many resonances can increase the desired nonlinear effect.

In this work we operated near the D-line atomic resonance of K to enhance the nonlinear response, similar to the previous works. The two resonance lines increase the nonlinear effect. Unlike the previous experiments on K vapor, an atomic system, we excited a molecule, KXe and generate SRS through the vibrational levels of the $A^2\Pi$ state. To the best of our knowledge, SRS has not been observed in this molecule or other alkali-rare gas systems. In this work, we generate stimulated emission on the Stokes generated wavelengths. These results from the molecular-optical interactions also allow for the experimental verification of the theoretical potential curves and results for the molecule KXe.

In the next chapter, the experimental setup is outlined, followed by the results and discussion in Chapter 3. Chapter 4 concludes the thesis and presents future directions for this project.

CHAPTER 2

EXPERIMENTAL SETUP

The experimental setup comprises three main components: the pump and probe, the gain medium, and the measurement equipment. The pump and probe sources are dye lasers pumped with a frequency doubled Q–switched Nd:YAG laser at a 10 Hz repetition rate and 8 ns pulses and the dye is LDS 765 in methanol. Both outputs are linearly polarized, with the probe vertically polarized and the pump horizontally polarized. The polarization of the pump and the probe are regulated by half waveplates with linear polarization denoting vertical polarization and circular polarization representing right-hand circular polarization. The energy of the lasers is controlled with a quarter wave plate and polarizing beam-splitter. The energy was measured with Coherent EnergyMax Sensors. The noise range of energy meters 1–3 in Figure 2.1 is <50 nJ and <1.2 µJ for energy meter 4. The linewidth of the dye laser is about 0.1 cm^{-1} at 625 nm according to the datasheet. This has not been experimentally verified. The wavelength of the dye laser has been verified using a Princeton Instruments Acton spectrometer and Pi-MAX4 camera calibrated with atomic lines.

Figure 2.1 is a general diagram of the setup which shows the pump and probe entering the oven and cell (the gain medium) from opposite directions. The energy of the pump and probe is measured with a pick-off window using pyroelectric energy meters, with the ratio determined during a cold-scan. Before entering the oven, a polarizing beam-splitter and quarter-waveplates are used to set the polarization.

The cell is fabricated by Precision Glass. Metallic K was placed inside and 300 Torr of Xe gas was added before the cell was sealed off for the gain medium in these experiments. The cell itself is a cylindrical 25.4 mm body made of quartz with angled windows at 11 degrees to prevent the formation of a Fabry–Pèrot cavity. In order to control the number density of K, the oven is heated. A cold finger is placed on the wall of the cell near the center,

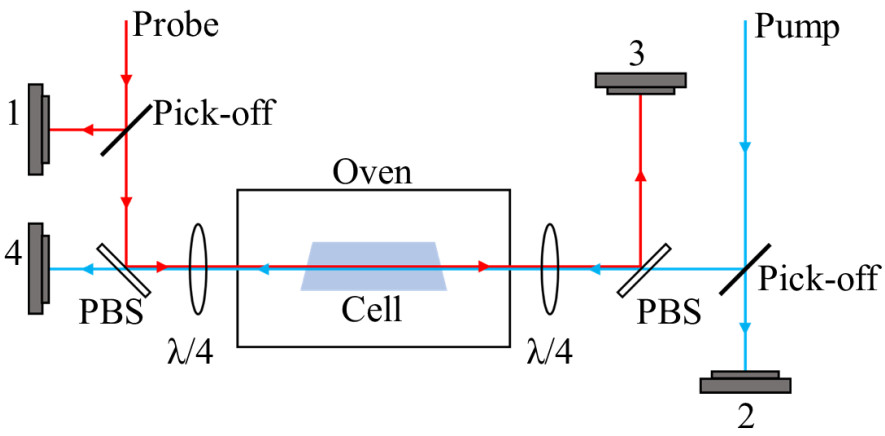

Figure 2.1: The experimental setup is shown above. The red and blue lines represent the probe and pump respectively and the labels 1–4 for the energy meters. The pick-off denotes a pick-off window. PBS and $\lambda/4$ are abbreviations for a polarizing beam-splitter and quarter-wave plate respectively.

allowing the windows of the cell to be about 5 degrees warmer preventing condensation of the alkali metal. In these experiments, the temperature was fixed at 493 K, resulting in the number density of K to be about 10^{15} cm^{-3}.

There are four main types of experiments performed for this amplifier system. The first is transmission scan, where the probe wavelength is scanned at a fixed energy. When the pump wavelength is scanned at a fixed energy, that scan is an amplified spontaneous emission (ASE) scan where the absorption can be measured. The last two experiments involve both the pump and the probe, one of which fixes the pump wavelength and scans the probe, pump–probe scan, and the other fixes the probe wavelength and scans the pump wavelength, an excitation scan. The delay between the pump and probe can be adjusted; however, for this work, the delay between the pump and the probe was fixed at 0.5 ns which corresponds to a 90% overlap of the pump and probe pulses.

CHAPTER 3

RESULTS AND DISCUSSION

In this chapter, the data collected from the experiments is presented and discussed in Sections 3.1 and 3.2. The analysis of the data is in Section 3.3.

3.1 Transmission and ASE Scans

The first set of data is from the transmission scans as shown in Figure 3.1 for both polarizations of the pump wavelength. The dips in the data represent the absorption of the probe corresponding to the D_2 and D_1 lines of 766.5 nm and 769.9 nm, respectively. These absorption peaks match the D line transitions in air on the NIST database [2]. As can be seen in Figure 3.1, there is some saturation present at the bottom of the dips; Figure A1 and Figure A2 show unsaturated data for both polarizations. In addition, Figure A1 has a second dip to the red of the D_1 line which can be attributed to a red satellite.

After confirming the D line resonances in the transmission scans, the next scan, an ASE scan, was performed to observe possible regions of gain. The results are shown in Figure 3.2 where the red and black curves represent circular and linear polarization of the pump, respectively. There are three features in this figure of great interest. The first is the dip at 766.5 nm (the D_2 line) which is associated with radiation trapping. The next feature is the broad ASE from the 766.5 nm pump for both polarizations indicating that the pump can be used to achieve gain in this medium. It will be shown experimentally that a significant portion of this pump energy is emitted on the D_1 line. The last feature is the second peak at 767 nm which is only observed with circular polarization.

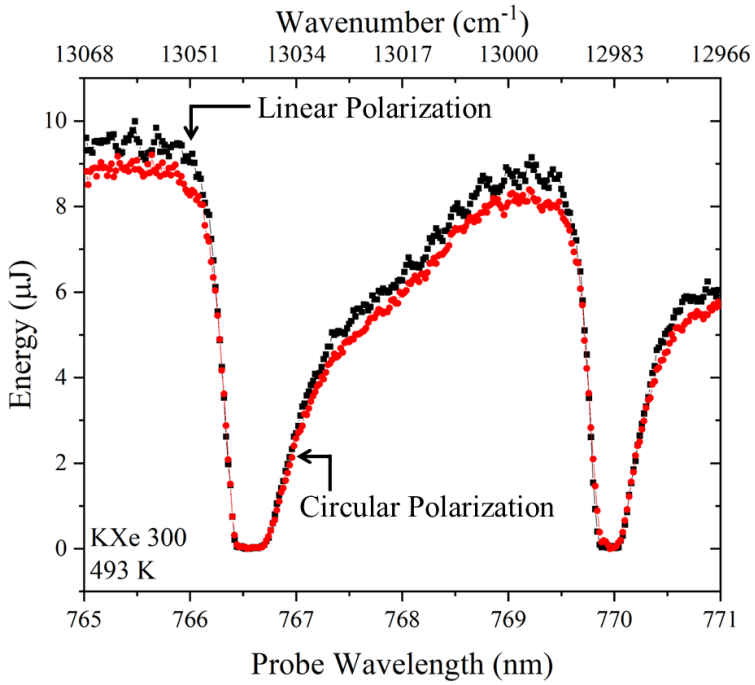

Figure 3.1: A plot of the transmission scan which determines where the resonances of KXe are in a specified range. The resonances found match the D line resonances of K. The red and black curves represent linear and circular polarization of the probe with their respective energies of 9.4 µJ and 9.0 µJ.

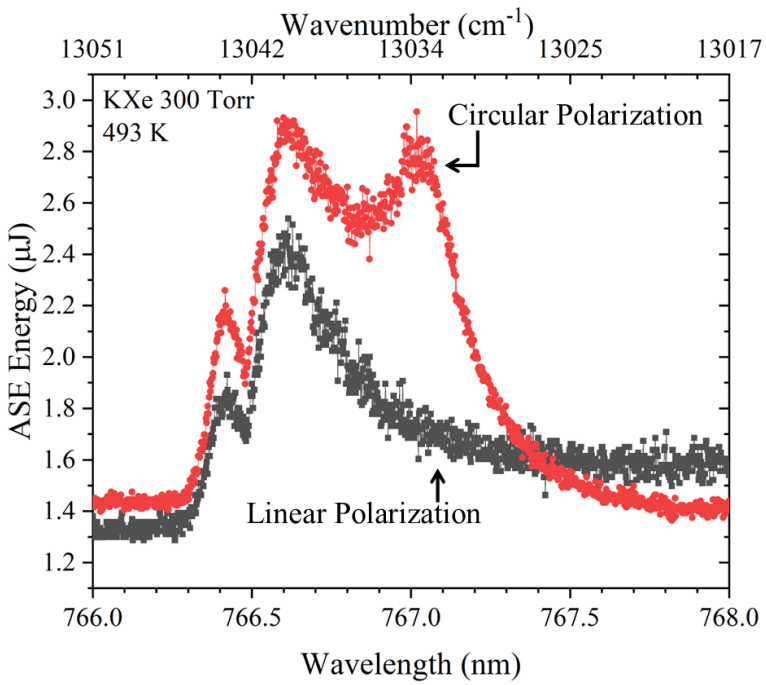

Figure 3.2: A plot of an ASE scan for the pump with linear (red) and circular (black) polarizations and their respective pulse energies of 19.9 mJ and 19.4 mJ. The ordinate represents the energy of the ASE.

3.2 Pump-Probe and Excitation Scans

Figures 3.3 and 3.4 are the results from the pump-probe scans for linearly and circularly polarized light. In these scans, the pump wavelength is fixed while scanning the probe which allows for the determination of where amplification of the probe occurs at a given pump wavelength. For example, we expect that when pumping on the D_2 line and probing on the D_1 line, there will be amplification on the D_1 line. This data also estimates how broad the transmission is on the D_1 resonance. In Figures 3.3 and 3.4, the pump-probe scans were repeated for several pump wavelengths. For each of these scans there are two peaks present for each pump. The first peak at 769.9 nm corresponds to the D_1 line of K as expected. This peak was present for all of the pump wavelengths tested, suggesting a broad transition for the pump. This was explored in the excitation scans which will be discussed later. Interestingly, the pump position at the D_2 line (766.5 nm) does not have the strongest amplification at the D_1 line. However, the energy for the second peak to the red of the D_2 line is comparable to that for the first. The integrated energy when pumping at 766.5 nm for both peaks is about the

same. As the pump wavelength moves to the red, the second peak observed in the pump-probe scans also moves to the red with lower amplification of the probe signal.

The energy difference between the pump wavelength and the probe wavelength for all the peaks is plotted in Figure 3.5 for both polarizations. As shown in Figure 3.5, there is no major difference between the polarizations of the pump and probe for the location of where probe amplification occurs. The data below the dashed line (the energy difference between the D_2 and D_1 line) is the energy difference between the pump and the peak on the D_1 resonance line. The pump wavelength of 766.5 nm does not produce the exact difference of 57.7 cm^{-1} due to the slight deviation of 0.02 nm (0.34 cm^{-1}) from the exact resonance line. The data above the dashed line is the energy difference between the pump and the second peak observed where the values vary around 60 cm^{-1}. This second peak is believed to be the result of molecular Raman which will be further discussed in Section 3.3.

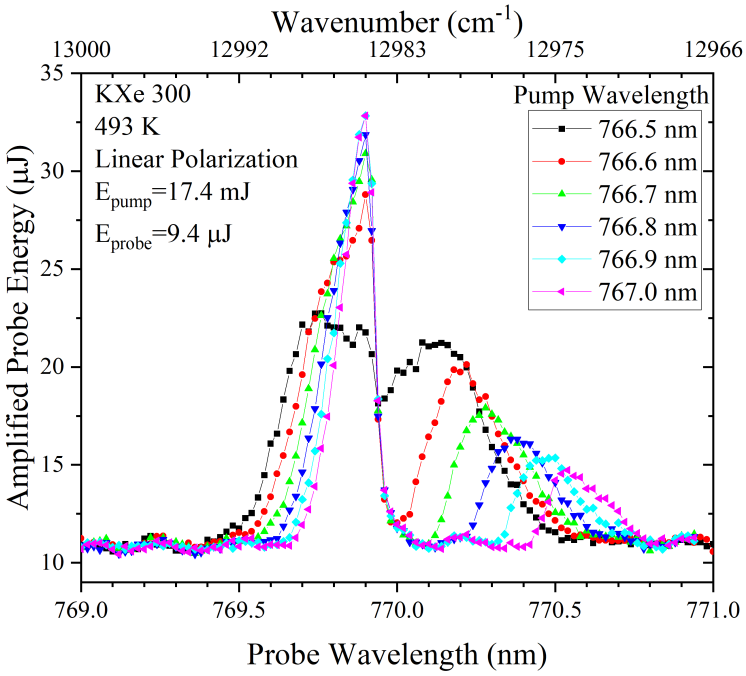

Figure 3.3: Pump-probe data for linearly polarized light. The pump and probe energy were 17.4 mJ and 9.4 µJ respectively. The peak on the left of the plot at 769.9 nm corresponds to the D_1 line which is amplified about three times due to the pump. The peaks to the red of the D_1 line move with the pump and have less amplification as the pump wavelength moves to the red.

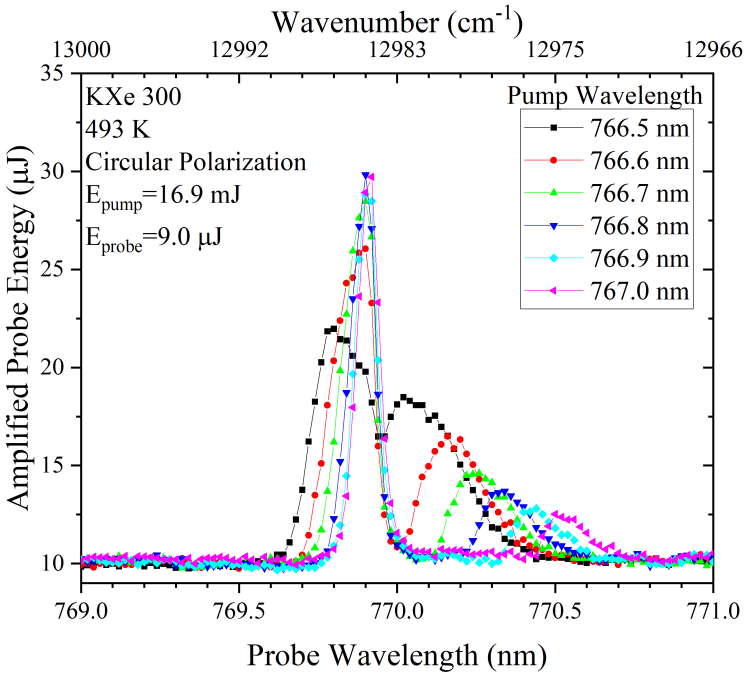

Figure 3.4: Pump-probe data for circularly polarized light. The pump and probe energy were 16.9 mJ and 9.0 µJ respectively. This data is very similar to the linear polarization shown in Fig. 3.3.

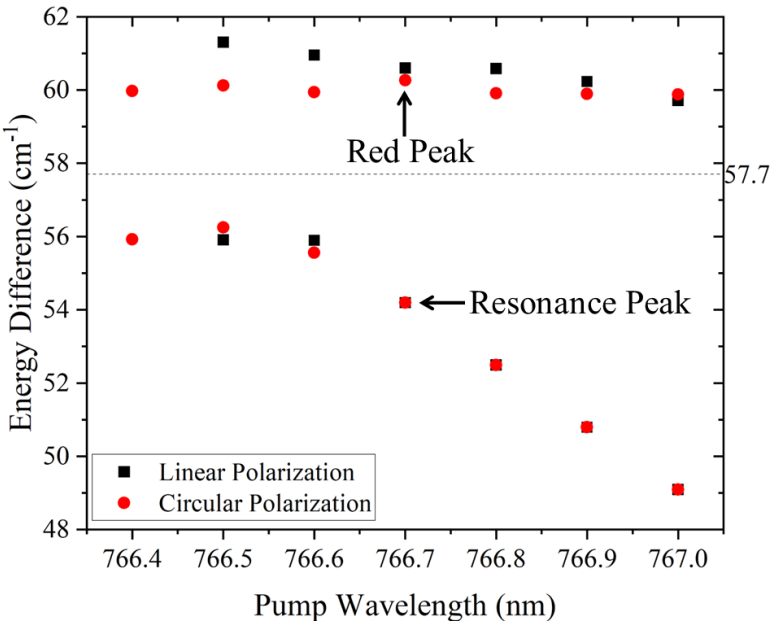

Figure 3.5: The energy difference between the pump wavelength and the peak of the probe wavelengths in Figs. 3.3 and A3 where the red and black represent circular and linear polarization. The dashed line at 57.7 cm^{-1} indicates the energy difference between the D_2 and D_1 line. The data below the dashed line labeled "resonance peak" represents the peak near the D_1 resonance line and the data above the dashed line labeled "red peak" represents the peak to the red of the D_1 line. The left peak data for wavelengths greater than 766.8 nm has no difference between the polarizations.

The last set of data collected was from the excitation scans where the probe wavelength is fixed and the pump is scanned. This scan was repeated for several probe energies for both linearly and circularly polarized light as shown in Figures 3.6 and 3.7. This data shows that as the probe wavelength is to the blue of the D_1 line, the pump wavelength is also shifted to the blue of the D_2 line. As the probe and pump wavelengths move closer to the D_1 line and D_2 line, the energy increases. When the probe wavelength is on the D_1 line (the orange curves in Figures 3.6 and 3.7), the FWHM of the pump wavelength doubles compared to the other pump wavelengths. In addition, the FWHM of the linear polarization data is about twice the FWHM of circular polarization data.

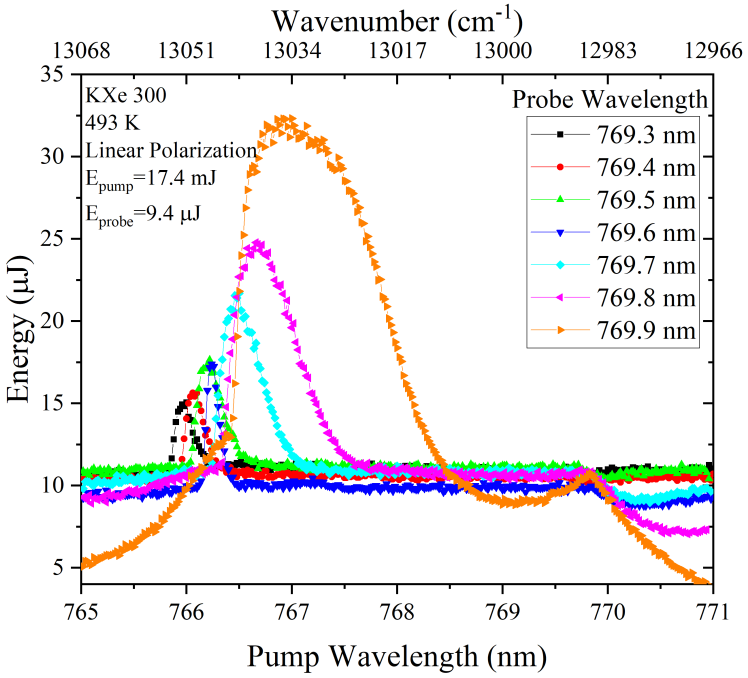

Figure 3.6: Excitation data for linearly polarized light. The pump and probe energy were 17.4 mJ and 9.4 µJ respectively.

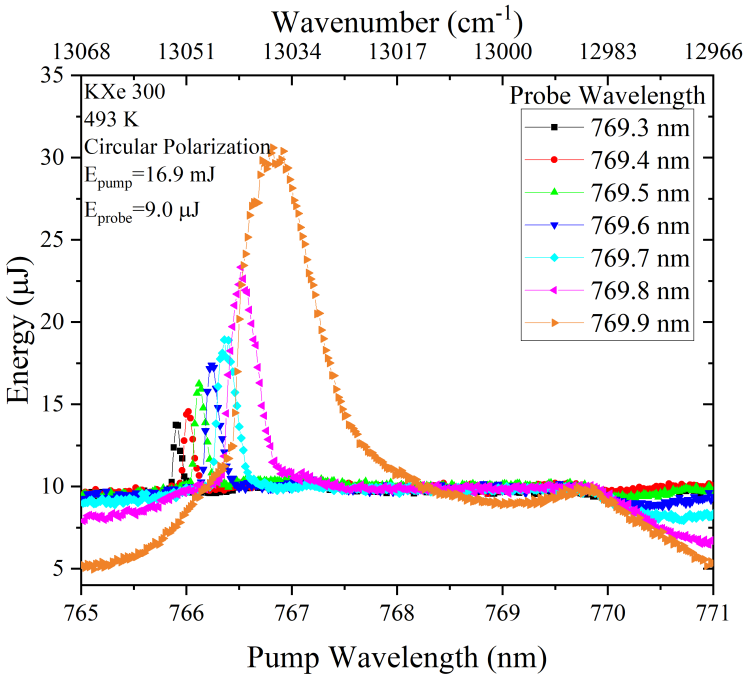

Figure 3.7: Excitation data for circularly polarized light. The pump and probe energy were 16.9 mJ and 9.0 µJ respectively. The FWHM for this data is reduced compared to Fig. 3.6.

3.3 Molecular Raman

In order to determine and verify the phenomena observed in the data presented above, the theoretical potential energy curves for KXe must be analyzed. One of the challenges for this system is the lack of theoretical data available. K is a much lighter atom than Rb and Cs, which have a lot of available theoretical data, so many of the approximations made for those systems may not be valid. For example, spin-orbit coupling for K is much smaller than for Rb and Cs when comparing it to the spin-free interactions [12]. There has been data found on KAr which could be used to estimate the curves for KXe, however, according to Baylis in his well-renowned 1969 paper, the well depths and reduced curvature for the $X^2\Sigma^+$, $A^2\Pi_{1/2,3/2}$, and $B^2\Sigma^+$ states are very different for KAr and KXe. For example, the well depth for the $A^2\Pi_{1/2,3/2}$ states is over three times deeper in KXe than in KAr [13].

Only one set of potential energy curves has been made available for KXe and the $A^2\Pi$ and $B^2\Sigma^+$ states from that dataset are plotted in Figure 3.8 where the red and blue data represent the $A^2\Pi$ and $B^2\Sigma^+$ states respectively.

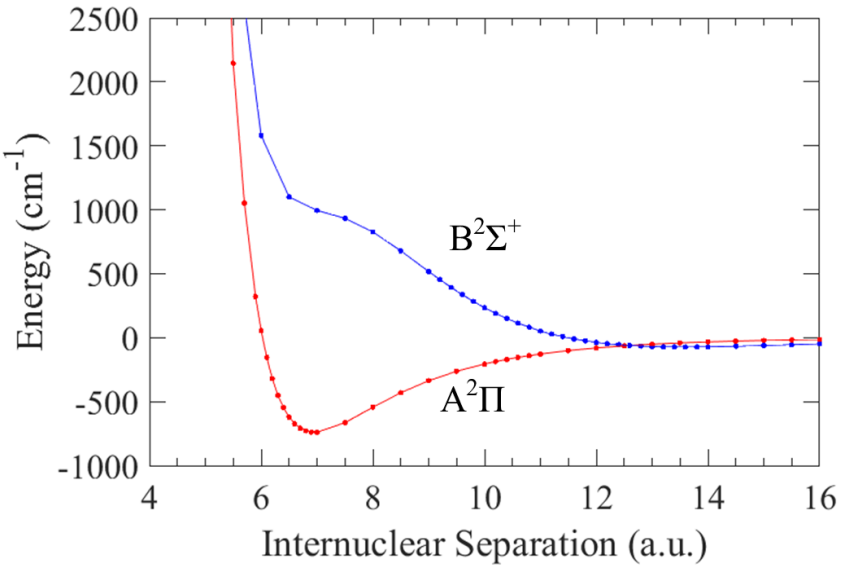

Figure 3.8: Potential energy curves for KXe where the red and blue data represent the $A^2\Pi$ and $B^2\Sigma^+$ states respectively. The raw data was taken from [12].

One interesting feature is the well in the $B^2\Sigma^+$ state which is located at 13.60 atomic units and has a dissociation energy of 73.1 cm^{-1}. This well depth is greater than the energy separation of the $4P_{3/2}$ and $4P_{1/2}$ levels (57.7 cm^{-1}) indicating that the $A^2\Pi$ and $B^2\Sigma^+$ curves intersect as can be seen in Figure 3.8. This intersection of the molecular potential energy curves along with the separation of the electronic states being much less than kT (343 cm^{-1}) indicates that energy transfer from the $B^2\Sigma^+$ to $A^2\Pi$ and from $4P_{3/2}$ and $4P_{1/2}$ is almost instantaneous.

From these potential energy curves, one can estimate the vibrational frequency of KXe by treating it as a harmonic oscillator [7]. The first step is to fit the curves to Equation 3.1 where E is the energy, k is the spring constant, and x is a position. The energy levels from Figure 3.8 were adjusted to have the bottom of the well positioned at 0 cm^{-1} and the center of the well positioned at 0 Å. The results of the curve fitting are shown in Figure 3.9.

$$E = \frac{1}{2}kx^2 \tag{3.1}$$

Using the spring constant extracted from the fits in Figure 3.9, the vi-

brational frequency of KXe can be calculated using Equation. 3.2 [7] where μ is the reduced mass. The vibrational frequencies were determined to be 60.8 cm^{-1} and 11.1 cm^{-1} for the $A^2\Pi$ and $B^2\Sigma^+$ states respectively.

$$\nu_{osc} = \frac{1}{2\pi}\sqrt{\frac{k}{\mu}} \tag{3.2}$$

The vibrational frequency calculated for the $A^2\Pi$ state is about 1 cm^{-1} off from the from frequency found in the pump-probe scans in Figure 3.5 for the right peaks of about 60 cm^{-1}. This strongly suggests that the second peak observed in the pump-probe scans is a result of molecular Raman. Normally, we would expect this from the $B^2\Sigma^+$, but because the $B^2\Sigma^+$ to $A^2\Pi$ states overlap it is possible to have vibrational Raman from the $A^2\Pi$ state. Assuming this is the case, the probe would stimulate the Stokes wavelength observed, suggesting that stimulated molecular Raman (SRS) is the main mechanism for the observed phenomenon.

It is important to note that the calculated vibrational frequency is close to the D_2 and D_1 separation. This could suggest that the phenomenon observed in the pump-probe scans is electronic. However, the broadening in the excitation scans for linear polarization suggests otherwise. The broadening observed in the linear polarization is much wider (around 30 cm^{-1}) than the other broadening mechanisms expected such as Doppler, resonance, and pressure broadening (each less than 0.2 cm^{-1}, calculations shown in Appendix A.2). The larger FWHM for linear polarization compared to circular polarization in the excitation scans is most likely from the molecular selection rules, since linear polarization can occupy more states than circular polarization. Further study of the molecular curves is required in order to determine the exact states involved in this process.

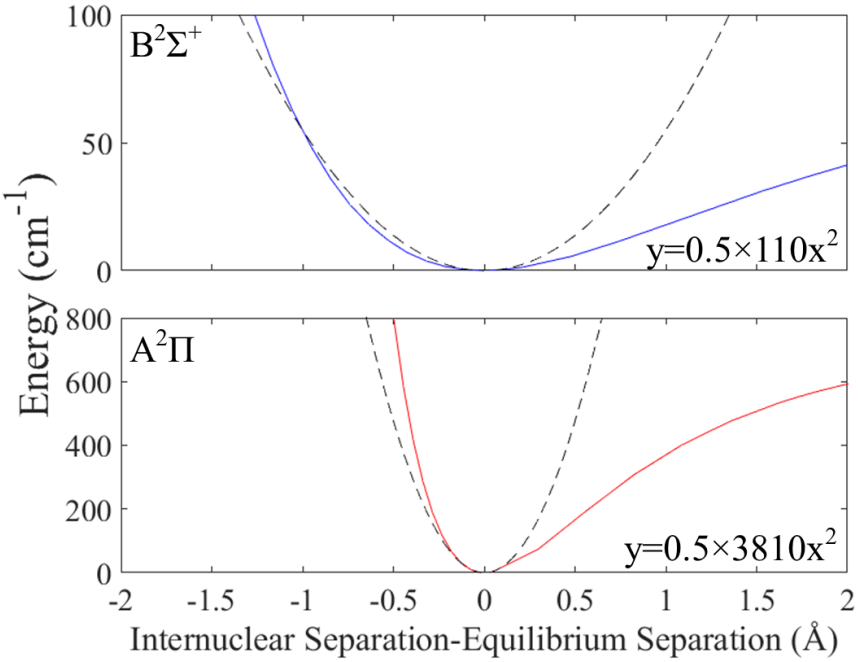

Figure 3.9: A fit for the potential energy curves from Fig. 3.8. Depending on the number of points chosen for the fitting, the constant for the $A^2\Pi$ state varies from 2870 to 3810 $cm^{-1}/Å^2$. The vibrational frequency reported is an average of these two values.

CHAPTER 4

CONCLUSIONS

The set of experiments discussed in this thesis demonstrate that KXe at 300 Torr has unique optical and molecular properties which have not been observed in other alkali rare gas molecules. For example, in this molecule and at this pressure, it is possible to achieve about three times gain on the D_1 line when pumping on the D_2 line. Population inversion in lower pressure Rb cells such as RbAr at 300 Torr has not been achieved when pumping on the D_2 line. In addition, molecular Raman has been observed during pump-probe experiments with the experimental vibrational frequency similar to the calculated one from theoretical potential energy curves of KXe. In addition, the optical effects observed have been confirmed to be molecular due to the broadening observed in the excitation scans.

A considerable amount of work is needed to confirm the results and understand the phenomena observed. One improvement is the vibrational frequency calculation. The dataset used is the only one available and has not been experimentally verified. While the $A^2\Pi$ state has a well depth and position similar to other renowned sources which do not provide the full energy curves, the $B^2\Sigma^+$ dissociation energy differs by about 400%. The accuracy of the $B^2\Sigma^+$ well depth is crucial due to the small energy difference of the electronic states. Without experimental verification, determining the best curves to use with the limited theoretical data is challenging. Some future approximations to make for these curves are to examine KAr, RbAr, and RbXe to try to predict the curves for KXe. Another method would be to personally perform the theoretical calculations. Alternatively, there are other methods to determine the vibrational frequency by treating KXe as an anharmonic oscillator. This can only be performed if higher-order vibrational modes can be determined experimentally. Determining the accurate potential curves is also crucial for calculating the Frank-Condon factor.

In addition to the potential energy curves, determining the selection rules

in KXe is a future goal to further understand how molecular Raman is occurring. Experimentally, future studies of KXe at higher pressures such as 1400 Torr are underway. The higher gas pressure increases the collision rate. In a high pressure cell, it might be possible to determine if a satellite structure is present. If a blue satellite of the D_2 line is present, a possible XPAL amplifier could be realized, which was the original goal of this work. These experiments will also be extended to other rare gases. Another challenge of working with K is that the K reacts away quickly. All the KXe cells used in this experiments have no more metallic K inside which occurred over a matter of months. Rb on the other hand can last for years. Currently, experiments are underway on low pressure Rb rare gas cells to determine if molecular Raman is possible which could provide another avenue for future study of molecular Raman in alkali-rare gas pairs.

While interesting physics has been experimentally realized in KXe at 300 Torr with some theoretical confirmation, there is still plenty of physics not understood or observed with this system. With the future work planned a more comprehensive picture can be realized from the phenomena observed in this current work.

APPENDIX A

SUPPLEMENTAL DATA AND CALCULATIONS

A.1 Additional Experimental Data

The first set of figures are additional transmission scans performed. In Figure A1, a shoulder was experimentally realized around 771.5 nm. Due to the fast reaction of K, this was not present in later scans. In addition, there was less absorption of the probe in this scan which better estimates the width of this transition line. The shoulder was not realized in circular polarization, but a scan with less saturating is shown in Figure A2.

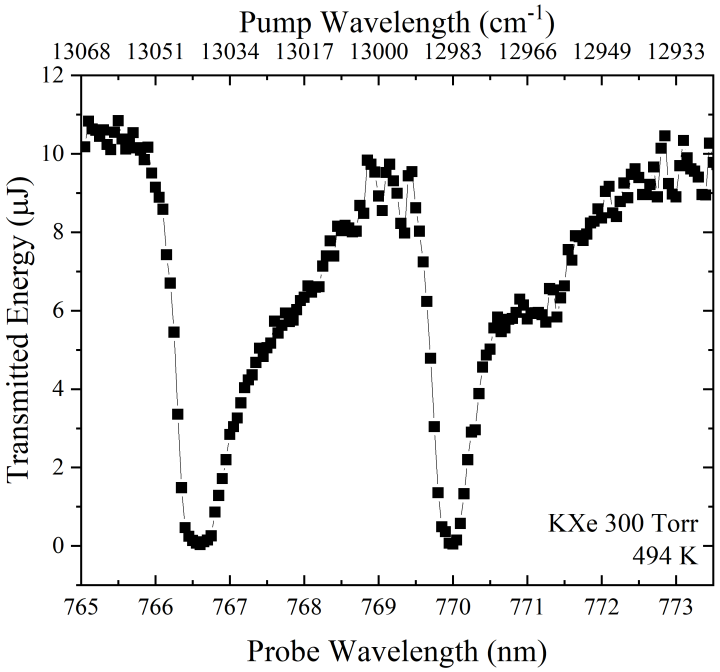

Figure A1: Transmission scan for linear polarization with the probe energy at 9.3 µJ.

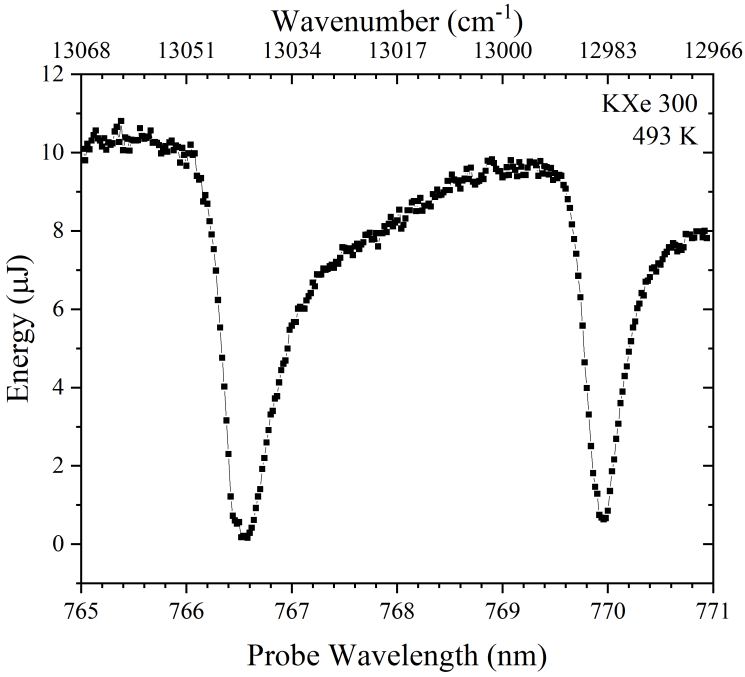

Figure A2: Transmission scan for circular polarization with the probe energy at 10.2 µJ.

An additional pump-probe scan for circular polarization is shown in Figure A3. This set of experiments includes a pump wavelength to the blue of the D_2 line which results in a dip at the D_1 line. There are still two peaks present.

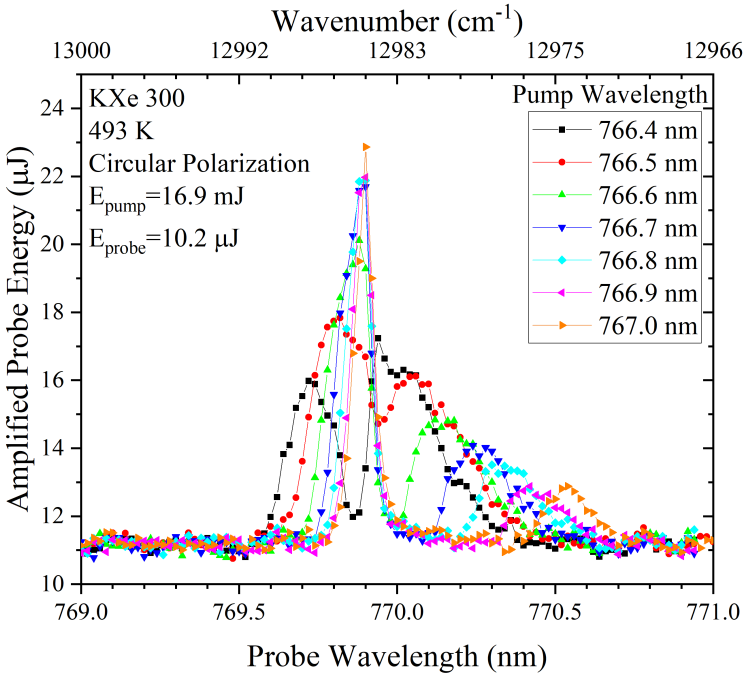

Figure A3: The pump-probe scan with the pump energy at 16.9 mJ and the probe energy at 10.2 µJ for circular polarization.

A.2 Broadening Calculations

There were three broadening calculations performed. The first is Doppler broadening as shown in Equation A.1 where λ is the wavelength, T is the temperature, and M is the atomic weight [14]. Using the values of 7680 Å, 493 K, and 39.1 AMU for the wavelength, temperature, and mass respectively, the Doppler broadening was calculated to be about 0.033 cm^{-1}.

$$\Delta\lambda_{1/2}^{D} = (7.16 \times 10^{-7})\lambda\sqrt{T/M} \tag{A.1}$$

The formula for resonance broadening was calculated using Equation A.2 [14] where g_i and g_j are the degeneracy of the states, λ is the observed wavelength, λ_r is the resonance wavelength, f_r is the oscillator strength, and N_i is the ground state number density. The degeneracies of the states are both 1 in this system. In this calculation, λ and λ_r were both set to be 7680 Å, due to the close observed lines for both resonances and f_r and N_i were 25 and 10^{15} cm^{-3} [2]. The resonance broadening was calculated to be about 0.2 cm^{-1}.

$$\Delta\lambda_{1/2}^{R} = 8.6 \times 10^{-30}\sqrt{g_i/g_k}\lambda^2\lambda_r f_r N_i \tag{A.2}$$

The pressure broadening was estimated using Equation A.3, where P is the pressure and was determined to be 0.2 cm^{-1} with a gas pressure of 300 Torr.

$$\Delta\nu \approx 20P \tag{A.3}$$

REFERENCES

[1] J. Readle, C. Wagner, J. Verdeyen, D. Carroll, and J. Eden, "Lasing in Cs at 894.3 nm pumped by the dissociate of CsAr excimers," *Electronics Letters*, vol. 44, 2008.

[2] "Strong lines of potassium(K)," https://physics.nist.gov/PhysRefData/Handbook/Tables/potassiumtable2.htm.

[3] J. D. Hewitt and J. G. Eden, "Lasing on the D lines of sodium pumped by free→free transitions of Na-Xe collision pairs," *Applied Physics Letters*, vol. 101, no. 24, p. 241109, 2012.

[4] B. Zhdanov, C. Maes, T. Ehrenreich, A. Havko, N. Koval, T. Meeker, B. Worker, B. Flusche, and R. Knize, "Optically pumped potassium vapor laser," in *Conference on Lasers and Electro-Optics/Quantum Electronics and Laser Science Conference and Photonic Applications Systems Technologies*. Optical Society of America, 2007, p. JWA83.

[5] J. Zweiback, G. Hager, and W. Krupke, "High efficiency hydrocarbon-free resonance transition potassium laser," *Optics Communications*, vol. 282, no. 9, pp. 1871–1873, 2009.

[6] B. Zhdanov, M. Rotondaro, M. Shaffer, and R. Knize, "Efficient potassium diode pumped alkali laser operating in pulsed mode," *Optics Express*, vol. 22, no. 14, pp. 17 266–17 270, Jul 2014.

[7] G. Herzberg, *Molecular Spectra and Molecular Structure*. Princeton, New Jersey: D. Van Nostrand Company, Inc., 1950, vol. I. Spectra of Diatomic Molecules.

[8] M. Rokni and S. Yatsiv, "Stimulated electronic Raman effect and parametric anti-Stokes radiation in potassium vapor," *IEEE Journal of Quantum Electronics*, vol. 3, no. 7, pp. 329–330, 1967.

[9] M. Rokni and S. Yatsiv, "Resonnace Raman effect in free atoms of potassium," *Physics Letters*, vol. 24A, no. 5, pp. 277–278, 1967.

[10] P. Sorokin, N. Shiren, J. Lankard, E. Hammond, and T. Kazyaka, "Stimulated electronic Raman scattering," *Applied Physics Letters*, vol. 10, no. 2, pp. 44–46, 1967.

[11] K. Brown, E. J. Hurd, J. Holtgrave, and G. Perram, "Stimulated electronic Raman and hyper-Raman scattering in potassium vapor," *Optics Communications*, vol. 309, pp. 21–25, 2013.

[12] E. Galbis, J. Douady, E. Jacquet, E. Giglio, and B. Gervais, "Potential energy cruves and spin-orbit coupling of light alkali-heavy rare gas molecules," *The Journal of Chemical Physics*, vol. 138, 2013.

[13] W. Baylis, "Semiempirical, pseudipotential calculation of alkali-noble-gas interatomic potentials," *The Journal of Chemical Physics*, vol. 51, pp. 2665–2679, 1969.

[14] "Atomic spectroscopy-Spectral line shapes, etc." https://www.nist.gov/pml/atomic-spectroscopy-compendium-basic-ideas-notation-data-and-formulas/atomic-spectroscopy-6.